


Article

Temperature Dependence of the Magnetic Properties of IrMn/CoFeB/Ru/CoFeB Exchange Biased Synthetic Antiferromagnets

Edoardo Albisetti *, Giuseppe Scaramuzzi, Christian Rinaldi, Matteo Cantoni, Riccardo Bertacco and Daniela Petti * 

Dipartimento di Fisica, Politecnico di Milano, Via Giuseppe Colombo 81, 20133 Milano, Italy; giuseppe.scaramuzzi@mail.polimi.it (G.S.); christian.rinaldi@polimi.it (C.R.); matteo.cantoni@polimi.it (M.C.); riccardo.bertacco@polimi.it (R.B.)

* Correspondence: edoardo.albisetti@polimi.it (E.A.); daniela.petti@polimi.it (D.P.)

Received: 21 December 2019; Accepted: 9 January 2020; Published: 14 January 2020



Abstract: Synthetic antiferromagnets (SAF) are widely used for a plethora of applications among which data storage, computing, and in the emerging field of magnonics. In this framework, controlling the magnetic properties of SAFs via localized thermal treatments represents a promising route for building novel magnonic materials. In this paper, we study via vibration sample magnetometry the temperature dependence of the magnetic properties of sputtered exchange bias SAFs grown via magnetron sputtering varying the ferromagnetic layers and spacer thickness. Interestingly, we observe a strong, reversible modulation of the exchange field, saturation field, and coupling strength upon heating up to 250 °C. These results suggest that exchange bias SAFs represent promising systems for developing novel artificial magnetic nanomaterials via localized thermal treatment.

Keywords: synthetic antiferromagnet; exchange bias; interlayer exchange coupling; vibrating sample magnetometry; CoFeB; thermally assisted magnetic scanning probe lithography; magnetron sputtering

1. Introduction

Synthetic antiferromagnets (SAFs) comprise ferromagnetic layers coupled antiferromagnetically through a non-magnetic spacer, by interlayer exchange coupling (IEC), which is essentially a Ruderman-Kittel-Kasuya-Yosida (RKKY) electronic coupling.

Starting from the first observation of the IEC in 1986 [1] and the subsequent study of the oscillatory behavior of IEC as a function of the spacer thickness [2,3], SAF systems played a fundamental role in the foundation of modern spintronics.

As in natural antiferromagnets, compensated SAFs present almost zero stray field and high stability. Furthermore, the interlayer coupling is typically orders of magnitude weaker than the exchange coupling between neighboring atoms in antiferromagnets, so that the manipulation of the magnetic order in SAF is easier. Some of the features that makes SAFs extremely interesting for applications is their wide applicability to in-plane as well out-of-plane magnetized materials, their large tunability via layer thickness and material composition, and the possibility to combine SAF and exchange bias by adding an antiferromagnetic layer to the stack. Throughout the years, SAFs were successfully used in spin-valves [4,5] and magnetic tunnel junctions [6–9] as reference layers, with applications as read heads in magnetoresistive [10,11] hard drives [12], magnetic random access memories (MRAM) [13–15], microwave oscillators [16] and magnetic biosensors [17–22]. More recently, SAFs have been proposed as base materials for racetrack memories [23], due to the higher domain wall velocity with respect to single ferromagnetic layers [24], and their capability to host a range of

topological spin-textures [25]. SAFs have also raised considerable interest in the growing field of magnonics [26,27], due to the peculiar properties of spin-waves propagating in antiferromagnetically coupled bilayers [28,29]. Furthermore, recently it has been demonstrated that localized thermal treatments in combination with magnetic fields can be effectively used for manipulating the static and dynamic magnetic properties of exchange bias systems [30–32]. In this framework, studying the temperature dependence of their magnetic properties is of crucial importance. In this work, we perform a systematic study of the magnetic properties of exchange biased SAF systems grown via magnetron sputtering, varying the ferromagnetic layers thickness (from 25 nm to 45 nm) and the spacer layer thickness (from 0.6 nm to 0.7 nm). In particular, we use vibration sample magnetometry (VSM), for measuring quantitatively the hysteresis loops as a function of the in-plane field angle and temperature, ranging from room temperature up to 250 °C. Then, from the hysteresis loops we extract the exchange field, saturation field, saturation magnetization and exchange constant, and study their dependence on temperature. This work sheds light on the temperature behavior of exchange biased synthetic antiferromagnets, allowing the design and implementation of novel methodologies for the thermally assisted control of their magnetic properties.

2. Materials and Methods

The samples were grown on Si/SiO₂ (100 nm) substrates by employing an AJA Orion8 magnetron sputtering system (AJA International, Scituate, MA, USA) with a base pressure below 1×10^{-8} Torr. All the materials were sputtered in the DC mode from single stoichiometric targets, using the parameters listed in Table 1. Note that two different conditions were employed for Ru: 3 mTorr for Ru films exploited as a capping layer and 5 mTorr for Ru films used as interlayer in the synthetic antiferromagnet. Indeed, the lower deposition rate at a pressure of 5 mTorr allows a better control on the Ru thickness, fundamental to obtain a sizable interlayer exchange coupling of the two ferromagnets.

Table 1. Magnetron sputtering parameters.

Material	Power (W)	Ar Pressure (mTorr)
Ru	50	3
Ru SAF	50	5
Co ₄₀ Fe ₄₀ B ₂₀	58	4
Ir ₂₂ Mn ₇₈	50	3

Before the deposition, the substrates underwent a soft etch in the same chamber at an Argon pressure of 3 mTorr and an RF power of 20 W for 5', in order to clean the surface. During the growth, a 30 mT magnetic field (H_G) was applied in the sample plane for setting the magnetocrystalline uniaxial anisotropy direction in the Co₄₀Fe₄₀B₂₀ layer and the exchange bias direction in the as-grown sample.

After the growth, the samples underwent an annealing at 250 °C for 5 min, which promoted the crystallization of the amorphous CoFeB and the IrMn layers.

Different sets of samples were studied, consisting of the stacks shown in Figure 1a, namely Si/SiO₂/Co₄₀Fe₄₀B₂₀ t /Ru d /Co₄₀Fe₄₀B₂₀ t /IrMn 10/Ru 2 (dimensions in nm) varying the thickness of the CoFeB ferromagnetic layers (t) and that of the non-magnetic interlayer Ru (d). The specific CoFeB and IrMn stoichiometry was chosen because of their widespread use in magnetic tunnel junctions, the low spin-wave damping in Co₄₀Fe₄₀B₂₀ and the high exchange bias strength. The exact composition of the studied samples is reported in Table 2, using the same coding which will be used in the subsequent discussion.

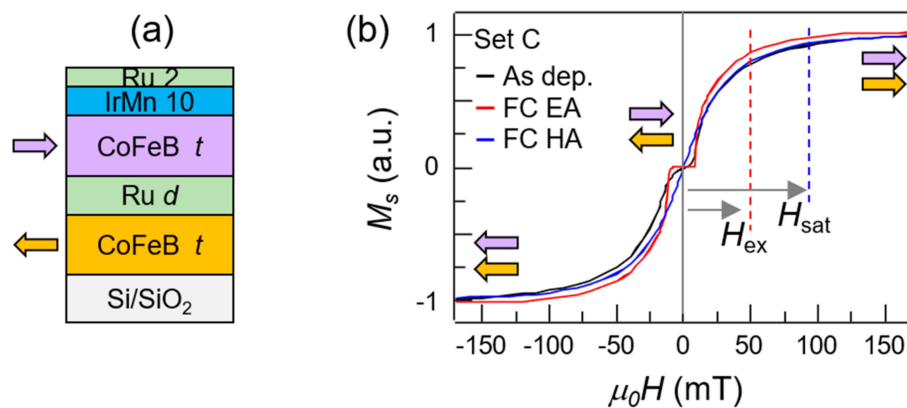


Figure 1. (a) Sketch of the CoFeB/Ru/CoFeB/IrMn/Ru synthetic antiferromagnet stacks grown via magnetron sputtering. t indicates the thickness of the CoFeB layers, ranging from 25 nm to 45 nm. d indicates the thickness of the Ru coupling layer, ranging from 0.6 to 0.7 nm; (b) room-temperature vibrating sample magnetometer hysteresis loop of sample C (CoFeB 35 nm, Ru 0.6 nm) in the as deposited sample measured along the easy axis (black line) and the sample after a field cooling at 250 °C measured along the easy axis (red line) and hard axis (blue line). The colored arrows indicate the direction of the magnetization of top (purple) and bottom (orange) layers. H_{ex} and H_{sat} indicate the exchange field and saturation field related to the annealed sample, respectively.

Table 2. List of the studied sample sets and corresponding stack compositions.

Set Name	Stack Compositions (Dimensions in nm)
A	Si/SiO ₂ /CoFeB 25/Ru 0.7/CoFeB 25/IrMn 10/Ru 2
B	Si/SiO ₂ /CoFeB 35/Ru 0.7/CoFeB 35/IrMn 10/Ru 2
C	Si/SiO ₂ /CoFeB 35/Ru 0.6/CoFeB 35/IrMn 10/Ru 2
D	Si/SiO ₂ /CoFeB 45/Ru 0.6/CoFeB 45/IrMn 10/Ru 2

The hysteresis loop of the films was measured via a vibrating sample magnetometer (VSM; EZ-9, Microsense, Lowell, MA, USA) as a function of the sample temperature, from RT to 250 °C, and of the direction of the magnetic field in the film plane. The VSM was used also for performing the initial annealing and field cooling of the samples.

3. Results and Discussion

3.1. Room-Temperature Magnetic Characterization and Angular Hysteresis Loops

Figure 1b shows the VSM hysteresis loops along the easy axis acquired at room temperature of set C (35 nm CoFeB, 0.6 nm Ru) for the as deposited sample, black line, and after the field cooling, red line. The field cooling was performed by heating the sample up to 250 °C and subsequently cooling it down to room temperature while applying a static 400 mT external magnetic field in the sample plane, in the same direction of the field applied during the growth, H_G . The field cooling sets the direction of the exchange bias, and therefore the pinning direction of the magnetization of the top CoFeB layer. The direction of the magnetization of the top (bottom) CoFeB layers as a function of the external field is indicated by the purple (orange) arrows. The hysteresis loop displays the characteristic plateau at low field, which is a signature of robust antiferromagnetic coupling between the two CoFeB layers, induced by the interlayer exchange coupling across the thin Ru layer. The plateau is also a signature of the presence of the anisotropy of the film, which is further confirmed by the angle-dependent measurement of Figure 2. The two main contributions are the magnetocrystalline anisotropy and the exchange bias set during the growth. The two lobes of the loop are related to the rotation of the top (negative fields) and bottom (positive fields) CoFeB layer. The saturation field H_{sat} and the exchange field H_{ex} are indicated in figure for the measurement after field cooling. In particular, H_{ex} was extracted from

the measurement as the halfway point between the end of the low-field plateau and the saturation field. In high external fields, the antiferromagnetic coupling is overcome by the Zeeman field, which saturates the magnetization in the direction of the applied field. Upon decreasing the magnetic field, the magnetizations rotate coherently and gradually reach the antiparallel alignment. The well-defined plateau in the annealed samples, with respect to the as-deposited samples, mainly arises from setting the unidirectional anisotropy of exchange bias via field cooling.

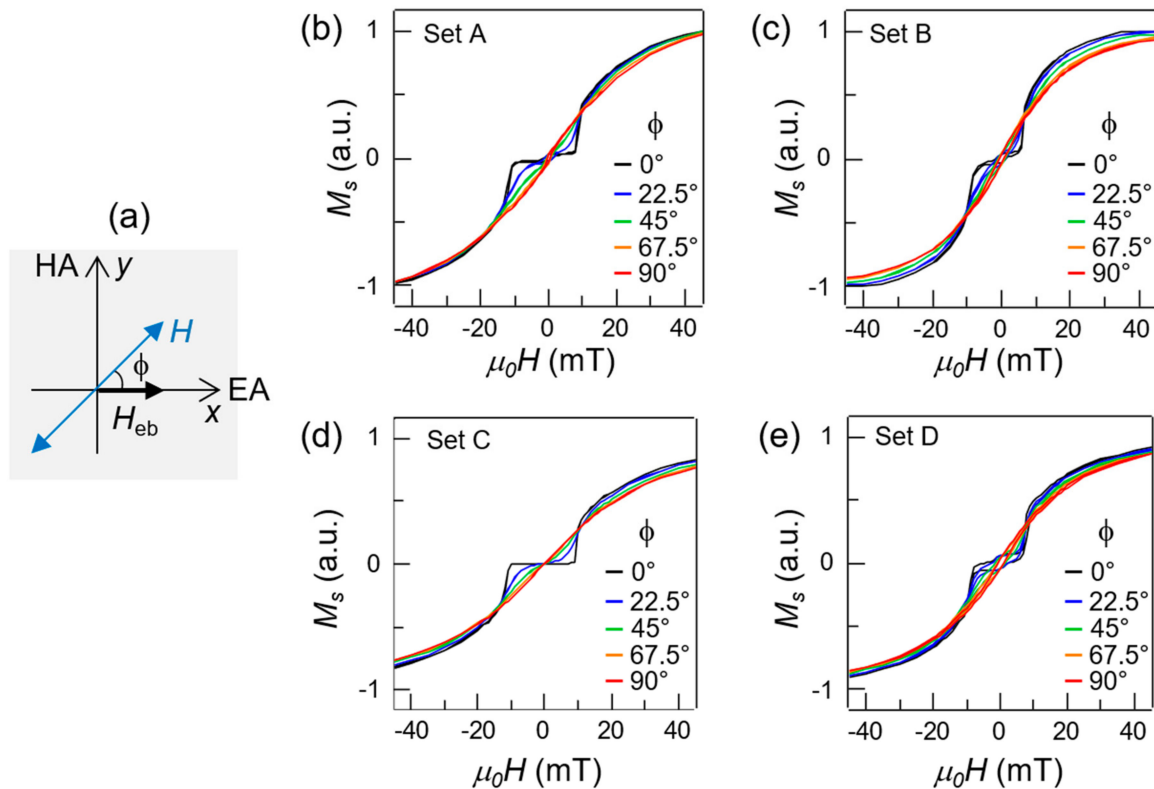


Figure 2. Room temperature hysteresis loops as a function of the field angle. (a) Sketch of the experimental configuration for the measurements. The thick arrows indicate the direction of the exchange bias field, set during field cooling (H_{eb}) along the x axis direction. ϕ indicates the angle of the external applied field (H) with respect to the exchange bias direction, in the plane of the film. (b–e) Hysteresis loops measured via vibration sample magnetometry (VSM) at room temperature as a function of the angle ϕ (color-coded) for set A, B, C, and D respectively.

Figure 2 shows the room temperature hysteresis loops after field cooling as a function of the angle of the external field applied in the plane of the sample. Panel (a) shows the geometry of the measurement. In particular, ϕ is the angle between the direction of the exchange bias H_{eb} , set during the field cooling, and the direction of the external field applied during the measurement H . Specifically, the easy magnetization axis (EA) is given by $\phi = 0^\circ$ and the hard axis (HA) is for $\phi = 90^\circ$. The measurements were performed in the same conditions on all the sets with a step of 22.5° from $\phi = 0^\circ$ to $\phi = 90^\circ$, color-coded. In all the sets, the loops feature the characteristic two lobes and low-field plateau along the EA, and the elongated loop along the HA. For intermediate angles, the loops assume a mixed EA and HA character, with the low field plateau progressively tilting to higher derivatives. Some samples show at low field a small hysteresis loop, probably due to slightly non-compensated ferromagnetic structures. The origin of non-compensation can be ascribed to the small variation of the CoFeB deposition conditions, or possibly to the influence of the surface roughness of one of the two ferromagnetic layers [33,34].

3.2. Temperature Dependence of the Magnetic Properties

Figure 3 shows the hysteresis loops of sets C and D along the easy axis ($\phi = 0^\circ$, panels (a–b)) and hard axis ($\phi = 90^\circ$, panels (c–d)), as a function of temperature, ranging from room temperature up to 250 °C, color-coded. Regarding the EA loops, three main effects of temperature are observed. First, a reduction of the plateau field with increasing temperature, from ~9 mT at room temperature down to ~4 mT at 250 °C in set C, and from ~7 mT at room temperature down to ~4 mT at 250 °C in set D. The decrease of the plateau was mainly due to the weakening of the unidirectional anisotropy set by the exchange bias while approaching the blocking temperature, combined with a reduction of the interlayer coupling strength, as the dependence of the magnetocrystalline anisotropy on the temperature in this ranges is much weaker [35]. Second, a reduction of the saturation field H_{sat} and exchange field H_{ex} , which was consistent with a reduction in the interlayer coupling with temperature. Third, as expected [36,37] we observe a slight reduction of the saturation magnetization M_s with increasing temperature. All these effects were however reversible, provided that the same exchange bias direction and strength was retrieved at the end of the heating process, e.g., (as performed in our experiments) by applying an external saturating field in the direction of the exchange bias during the cooling process.

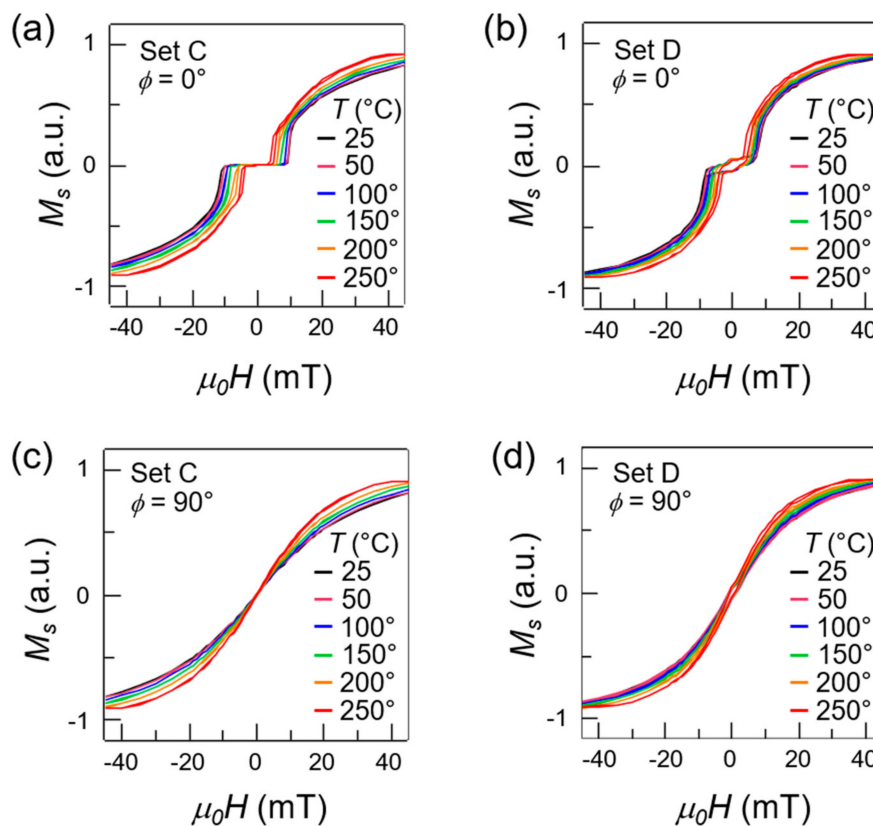


Figure 3. (a,b) Hysteresis loops of set C and set D along the easy-axis ($\phi = 0^\circ$) measured as a function of temperature (color-coded) ranging from 25 °C to 250 °C; (c,d) Hysteresis loops of set C and set D along the hard-axis ($\phi = 90^\circ$) measured as a function of temperature (color-coded) ranging from 25 °C to 250 °C.

For analyzing quantitatively the characteristics of the hysteresis loops, in Figure 4 we plotted the exchange field H_{ex} (a) and saturation field H_{sat} (b) as a function of the temperature for all the sample sets (A–D). From the room temperature data (at $T = 25^\circ\text{C}$) of both panel (a) and panel (b), we observed higher H_{ex} around 45 mT and H_{sat} around 85 mT in sets C–D, and lower H_{ex} around 20 mT and H_{sat} around 40 mT in sets A–B. This was consistent with the oscillatory nature of the interlayer coupling as

a function of the Ru thickness, which was 0.6 nm in sets C–D and 0.7 nm in sets A–B. It is worth noting that, the Ru thickness being equal, slightly higher exchange and saturation fields were observed in the sets characterized by thinner CoFeB layers (set A, 25 nm and set C, 35 nm). This is coherent with the interfacial nature of the antiferromagnetic interlayer coupling, which is inversely proportional to the film thickness.

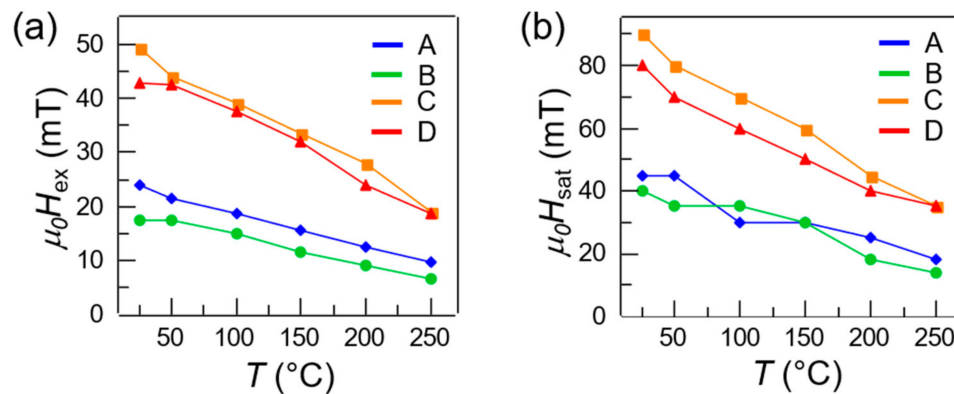


Figure 4. (a,b) Exchange field $\mu_0 H_{ex}$ and saturation field $\mu_0 H_{sat}$ as a function of temperature for sets A–D (color-coded).

Regarding the temperature dependence of the exchange and saturation fields, we observed an overall reduction of both parameters with increasing temperature, in all sample sets. In particular, both H_{ex} and H_{sat} displayed a reduction of about 60% from room temperature to 250 °C. This behavior is particularly interesting in the framework of thermally assisted magnetic writing schemes, such as TAMR (thermally assisted magnetic recording) or tam-SPL (thermally assisted magnetic scanning probe lithography), where local heating in combination with external fields is used for writing magnetization patterns. Note that, at the same time, the reduction of the plateau field was around 50%.

In Figure 5, we studied the saturation magnetization (a) and the interlayer coupling strength (b) as a function of temperature. M_s measured at room temperature is $0.9\text{--}1.1 \times 10^6$ A/m in all sets, which is in agreement with values found in the literature [38,39] for CoFeB films with the same stoichiometry. The M_s , which lowers with increasing temperature due to magnon excitation [40], was calculated normalizing the quantitative VSM measurements by the magnetic volume of each sample. The slight variations observed across different samples are due to non-idealities in the sample shape. In order to study the dependence of the coupling coefficient on the temperature, we calculated the total effective coupling strength $J_{eff} = H_{ex} M_s t$, where H_{ex} is the exchange field (see Figure 1b), M_s is the saturation magnetization and t is the sample thickness. The physical origin of such dependence can be ascribed to both interfacial effects, spacer-related mechanisms or effects arising in the magnetic layers [41]. In panel (b) we plot J_{eff} as a function of temperature for all the sets. As previously noted, sets A and B (Ru 0.7 nm thick) feature a lower $J_{eff} \sim 1.25$ mJ/m² with respect to sets C and D (Ru 0.6 nm thick), which feature $J_{eff} \sim 3.5$ mJ/m² at room temperature, due to the different Ru interlayer thickness, consistently with the expected oscillatory behavior [2]. Noteworthy, J_{eff} was reduced reversibly by 60–65% from room temperature to 250 °C with only slight variations across different sets, suggesting that even mild heating treatment could significantly and temporarily alter the SAF coupling strength, with high potential for applications. These results were consistent with those found in similar system, namely synthetic antiferromagnets based on thin ferromagnetic layers with in plane and perpendicular to the plane magnetic anisotropies [35,42]. The theoretical explanation of the decrease of interlayer exchange coupling with the temperature can be found in [41].

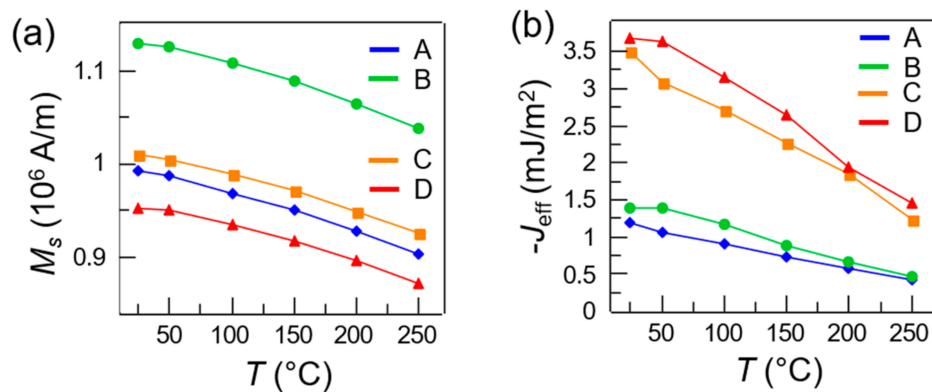


Figure 5. (a) Saturation magnetization M_s as a function of temperature for set A–D (color-coded); (b) Coupling strength J_{eff} as a function of temperature for set A–D (color-coded).

4. Conclusions

In this work, we studied the temperature and angular dependence of the magnetic properties of exchange biased synthetic antiferromagnets, in the case of compensated in-plane magnetized layers with thickness ranging from 25 nm to 45 nm. Noteworthy, we observed a strong reversible reduction of the exchange field, saturation field and antiferromagnetic coupling strength with a mild heating treatment (up to 250 °C). These results are particularly interesting in the framework of heat-assisted magnetic writing methods such as thermally assisted magnetic scanning probe lithography (tam-SPL), where localized heating in combination with external fields were used for reversibly writing the magnetic properties of thin-film materials. These results suggest that SAFs represent promising systems for developing novel artificial magnetic nanomaterials via localized thermal treatment.

Author Contributions: Conceptualization, data analysis and writing E.A., D.P.; Experiments E.A., G.S., C.R., M.C., D.P. Supervision, R.B. All authors have read and agreed to the published version of the manuscript.

Funding: The research leading to these results has received funding from the European Union’s Horizon 2020 research and innovation program under grant agreements no. 705326, project SWING.

Conflicts of Interest: The authors declare no conflict of interest.

References

1. Grünberg, P.; Schreiber, R.; Pang, Y. Layered Magnetic Structures: Evidence for Antiferromagnetic Coupling of Fe Layers across Cr Interlayers. *Phys. Rev. Lett.* **1986**, *57*, 2442–2445. [[CrossRef](#)] [[PubMed](#)]
2. Parkin, S.S.P.; More, N.; Roche, K.P. Oscillations in exchange coupling and magnetoresistance in metallic superlattice structures: Co/Ru, Co/Cr, and Fe/Cr. *Phys. Rev. Lett.* **1990**, *64*, 2304–2307. [[CrossRef](#)] [[PubMed](#)]
3. Bruno, P.; Chappert, C. Oscillatory coupling between ferromagnetic layers separated by a nonmagnetic metal spacer. *Phys. Rev. Lett.* **1991**, *67*, 1602–1605. [[CrossRef](#)] [[PubMed](#)]
4. Dieny, B.; Speriosu, V.S.; Gurney, B.A.; Parkin, S.S.P.; Wilhoit, D.R.; Roche, K.P.; Metin, S.; Peterson, D.T.; Nadimi, S. Spin-valve effect in soft ferromagnetic sandwiches. *J. Magn. Magn. Mater.* **1991**, *93*, 101–104. [[CrossRef](#)]
5. Kerr, E.; van Dijken, S.; Coey, J.M.D. Influence of the annealing field strength on exchange bias and magnetoresistance of spin valves with IrMn. *J. Appl. Phys.* **2005**, *97*, 093910. [[CrossRef](#)]
6. Yuasa, S.; Djayaprawira, D.D. Giant tunnel magnetoresistance in magnetic tunnel junctions with a crystalline MgO(0 0 1) barrier. *J. Phys. D: Appl. Phys.* **2007**, *40*, R337–R354. [[CrossRef](#)]
7. Zaleski, A.; Skowronski, W.; Czapkiewicz, M.; Kanak, J.; Stobiecki, T.; Macedo, R.; Cardoso, S.; Freitas, P.P. Reduction of critical current in magnetic tunnel junctions with CoFeB/Ru/CoFeB synthetic free layer. *J. Phys. Conf. Ser.* **2010**, *200*, 052035. [[CrossRef](#)]
8. Cuchet, L.; Rodmacq, B.; Auffret, S.; Sousa, R.C.; Prejbeanu, I.L.; Dieny, B. Perpendicular magnetic tunnel junctions with a synthetic storage or reference layer: A new route towards Pt- and Pd-free junctions. *Sci. Rep.* **2016**, *6*, 21246. [[CrossRef](#)]

9. Lee, Y.M.; Hayakawa, J.; Ikeda, S.; Matsukura, F.; Ohno, H. Giant tunnel magnetoresistance and high annealing stability in CoFeB/MgO/CoFeB magnetic tunnel junctions with synthetic pinned layer. *Appl. Phys. Lett.* **2006**, *89*, 87–90. [[CrossRef](#)]
10. Baibich, M.N.; Broto, J.M.; Fert, A.; Van Dau, F.N.; Petroff, F.; Etienne, P.; Creuzet, G.; Friederich, A.; Chazelas, J. Giant Magnetoresistance of (001)Fe/(001)Cr Magnetic Superlattices. *Phys. Rev. Lett.* **1988**, *61*, 2472–2475. [[CrossRef](#)]
11. Binasch, G.; Grünberg, P.; Saurenbach, F.; Zinn, W. Enhanced magnetoresistance in layered magnetic structures with antiferromagnetic interlayer exchange. *Phys. Rev. B* **1989**, *39*, 4828–4830. [[CrossRef](#)] [[PubMed](#)]
12. Childress, J.R.; Carey, M.J.; Wilson, R.J.; Smith, N.; Tsang, C.; Ho, M.K.; Carey, K.; Macdonald, S.A.; Ingall, L.M.; Gurney, B.A. IrMn Spin-Valves for High Density Recording. *IEEE Trans. Magn.* **2001**, *37*, 1745–1748. [[CrossRef](#)]
13. Parkin, S.; Jiang, X.; Kaiser, C.; Panchula, A.; Roche, K.; Samant, M. Magnetically engineered spintronic sensors and memory. *Proc. IEEE* **2003**, *91*, 661–680. [[CrossRef](#)]
14. Bhatti, S.; Sbiaa, R.; Hirohata, A.; Ohno, H.; Fukami, S.; Piramanayagam, S.N. Spintronics based random access memory: A review. *Mater. Today* **2017**, *20*, 530–548. [[CrossRef](#)]
15. Smith, N.; Maat, S.; Carey, M.J.; Childress, J.R. Coresonant Enhancement of Spin-Torque Critical Currents in Spin Valves with a Synthetic-Ferrimagnet Free Layer. *Phys. Rev. Lett.* **2008**, *101*, 247205. [[CrossRef](#)]
16. Hrkac, G.; Keatley, P.S.; Bryan, M.T.; Butler, K. Magnetic vortex oscillators. *J. Phys. D. Appl. Phys.* **2015**, *48*, 453001. [[CrossRef](#)]
17. Search, H.; Journals, C.; Contact, A.; Iopscience, M.; Address, I.P.; Freitas, P.P.; Ferreira, R.; Cardoso, S.; Cardoso, F. Magnetoresistive sensors. *J. Phys. Condens. Matter* **2007**, *19*, 165221.
18. Gaster, R.S.; Xu, L.; Han, S.-J.; Wilson, R.J.; Hall, D.A.; Osterfeld, S.J.; Yu, H.; Wang, S.X. Quantification of protein interactions and solution transport using high-density GMR sensor arrays. *Nat. Nanotechnol.* **2011**, *6*, 314–320. [[CrossRef](#)]
19. Donolato, M.; Sogne, E.; Dalslet, B.T.; Cantoni, M.; Petti, D.; Cao, J.; Cardoso, F.; Cardoso, S.; Freitas, P.P.; Hansen, M.F.; et al. On-chip measurement of the Brownian relaxation frequency of magnetic beads using magnetic tunneling junctions. *Appl. Phys. Lett.* **2011**, *98*, 073702. [[CrossRef](#)]
20. Sharma, P.; Albisetti, E.; Monticelli, M.; Bertacco, R.; Petti, D. Exchange Bias Tuning for Magnetoresistive Sensors by Inclusion of Non-Magnetic Impurities. *Sensors* **2016**, *16*, 1030. [[CrossRef](#)]
21. Sharma, P.P.; Albisetti, E.; Massetti, M.; Scolari, M.; La Torre, C.; Monticelli, M.; Leone, M.; Damin, F.; Gervasoni, G.; Ferrari, G.; et al. Integrated platform for detecting pathogenic DNA via magnetic tunneling junction-based biosensors. *Sens. Actuators B Chem.* **2017**, *242*, 280–287. [[CrossRef](#)]
22. Albisetti, E.; Petti, D.; Damin, F.; Cretich, M.; Torti, A.; Chiari, M.; Bertacco, R. Photolithographic bio-patterning of magnetic sensors for biomolecular recognition. *Sens. Actuators B Chem.* **2014**, *200*, 39–46. [[CrossRef](#)]
23. Parkin, S.S.P.; Hayashi, M.; Thomas, L. Magnetic Domain-Wall Racetrack Memory. *Science* **2008**, *320*, 190–194. [[CrossRef](#)] [[PubMed](#)]
24. Yang, S.H.; Ryu, K.S.; Parkin, S. Domain-wall velocities of up to 750 m s⁻¹ driven by exchange-coupling torque in synthetic antiferromagnets. *Nat. Nanotechnol.* **2015**, *10*, 221–226. [[CrossRef](#)]
25. Legrand, W.; Maccariello, D.; Ajejas, F.; Collin, S.; Vecchiola, A.; Bouzehouane, K.; Reyren, N.; Cros, V.; Fert, A. Room-temperature stabilization of antiferromagnetic skyrmions in synthetic antiferromagnets. *Nat. Mater.* **2019**, *19*, 34–42. [[CrossRef](#)]
26. Chumak, A.V.; Vasyuchka, V.I.; Serga, A.A.; Hillebrands, B. Magnon spintronics. *Nat. Phys.* **2015**, *11*, 453–461. [[CrossRef](#)]
27. Lenk, B.; Ulrichs, H.; Garbs, F.; Münzenberg, M. The building blocks of magnonics. *Phys. Rep.* **2011**, *507*, 107–136. [[CrossRef](#)]
28. Sluka, V.; Schneider, T.; Gallardo, R.A.; Kákay, A.; Weigand, M.; Warnatz, T.; Mattheis, R.; Roldán-Molina, A.; Landeros, P.; Tiberkevich, V.; et al. Emission and propagation of 1D and 2D spin waves with nanoscale wavelengths in anisotropic spin textures. *Nat. Nanotechnol.* **2019**, *14*, 328–333. [[CrossRef](#)]
29. Albisetti, E.; Tacchi, S.; Silvani, R.; Scaramuzzi, G.; Finizio, S.; Wintz, S.; Wintz Rinaldi, C.; Cantoni, M.S.; Raabe, J.; Carlotti, G.; et al. Optically-inspired nanomagnonics with nonreciprocal spin waves in synthetic antiferromagnets. *Adv. Mater.* **2020**. [[CrossRef](#)]

30. Albisetti, E.; Petti, D.; Pancaldi, M.; Madami, M.; Tacchi, S.; Curtis, J.; King, W.P.; Papp, A.; Csaba, G.; Porod, W.; et al. Nanopatterning reconfigurable magnetic landscapes via thermally assisted scanning probe lithography. *Nat. Nanotechnol.* **2016**, *11*, 545–551. [[CrossRef](#)]
31. Albisetti, E.; Petti, D.; Sala, G.; Silvani, R.; Tacchi, S.; Finizio, S.; Wintz, S.; Calò, A.; Zheng, X.; Raabe, J.; et al. Nanoscale spin-wave circuits based on engineered reconfigurable spin-textures. *Commun. Phys.* **2018**, *1*, 56. [[CrossRef](#)]
32. Albisetti, E.; Calò, A.; Spieser, M.; Knoll, A.W.; Riedo, E.; Petti, D. Stabilization and control of topological magnetic solitons via magnetic nanopatterning of exchange bias systems. *Appl. Phys. Lett.* **2018**, *113*, 162401. [[CrossRef](#)]
33. Desai, M.; Misra, A.; Doyle, W.D. Effect of interface roughness on exchange coupling in synthetic antiferromagnetic multilayers. *IEEE Trans. Magn.* **2005**, *41*, 3151–3153. [[CrossRef](#)]
34. Varvaro, G.; Laureti, S.; Peddis, D.; Hassan, M.; Barucca, G.; Mengucci, P.; Gerardino, A.; Giovine, E.; Lik, O.; Nissen, D.; et al. Co/Pd-Based synthetic antiferromagnetic thin films on Au/resist underlayers: Towards biomedical applications. *Nanoscale* **2019**, *11*, 21891–21899. [[CrossRef](#)] [[PubMed](#)]
35. Wiese, N.; Dimopoulos, T.; Rührig, M.; Wecker, J.; Reiss, G.; Sort, J.; Nogués, J. Strong temperature dependence of antiferromagnetic coupling in CoFeB/Ru/CoFeB. *Europhys. Lett.* **2007**, *78*, 67002. [[CrossRef](#)]
36. Callen, H.B.; Callen, E. The present status of the temperature dependence of magnetocrystalline anisotropy, and the power law. *J. Phys. Chem. Solids* **1966**, *27*, 1271–1285. [[CrossRef](#)]
37. Sato, H.; Chureemart, P.; Matsukura, F.; Chantrell, R.W.; Ohno, H.; Evans, R.F.L. Temperature-dependent properties of CoFeB/MgO thin films: Experiments versus simulations. *Phys. Rev. B* **2018**, *98*, 214428. [[CrossRef](#)]
38. Chen, Y.-T.; Xie, S.M. Magnetic and Electric Properties of Amorphous Co₄₀Fe₄₀B₂₀ Thin Films. *J. Nanomater.* **2012**, *2012*, 29. [[CrossRef](#)]
39. Conca, A.; Greser, J.; Sebastian, T.; Klingler, S.; Obry, B.; Leven, B.; Hillebrands, B. Low spin-wave damping in amorphous Co₄₀Fe₄₀B₂₀ thin films. *J. Appl. Phys.* **2013**, *113*, 213909. [[CrossRef](#)]
40. Bloch, F. Zur Theorie des Ferromagnetismus. *Z. Phys. A Hadron. Nucl.* **1930**, *61*, 206–219. [[CrossRef](#)]
41. Schwieger, S.; Nolting, W. Origin of the temperature dependence of interlayer exchange coupling in metallic trilayers. *Phys. Rev. B* **2004**, *69*, 224413. [[CrossRef](#)]
42. Li, Y.; Jin, X.; Pan, P.; Tan, F.N.; Lew, W.S.; Ma, F. Temperature-dependent interlayer exchange coupling strength in synthetic antiferromagnetic [Pt/Co]₂/Ru/[Co/Pt]₄ multilayers. *Chin. Phys. B* **2018**, *27*, 127502. [[CrossRef](#)]

